ELSEVIER

Contents lists available at ScienceDirect

Chemical Engineering Journal

journal homepage: www.elsevier.com/locate/cej





Airlift Taylor Flow bioreactors as a novel platform to enhance H₂-assisted CO₂ bioconversion processes

Pedro Cruz ^{a,b,c}, Raquel Lebrero ^{a,b}, Alberto Vergara-Fernández ^c, Raúl Muñoz ^{a,b,*}

- ^a Institute of Sustainable Processes, University of Valladolid, Dr. Mergelina, s/n, 47011 Valladolid, Spain
- b Department of Chemical and Environmental Engineering, University of Valladolid, Dr. Mergelina, s/n, 47011 Valladolid, Spain
- c Green Technology Research Group, Facultad de Ingeniería y Ciencias Aplicadas, Universidad de Los Andes, 7550000 Santiago, Chile

ABSTRACT

The microbial valorization of CO_2 requires the development of novel bioreactor configurations capable of ensuring a cost-effective gas-liquid mass transfer. This study presents the design, characterization and performance evaluation of a novel Airlift Taylor Flow Reactor (ATFR), which integrates the gas-induced liquid recirculation of airlift systems, with the high gas-liquid mass transfer potential of Taylor flow in multicapillary systems. The liquid recirculation flow in the downcomer was quantified using a colour tracer method, and the volumetric oxygen mass transfer coefficient ($k_L a$) was determined via the sulphite oxidation method, both with and without forced recirculation. The results showed that the implementation of forced mechanical recirculation via a centrifugal pump negatively impacted the total liquid recirculation and $k_L a$. A maximum $k_L a$ of $891 \pm 23 \ h^{-1}$ was achieved at a gas flow rate of $60 \ L \ min^{-1}$, representing a $75 \ \%$ increase compared to the same condition with external forced liquid recirculation. The autotrophic growth of *Cupriavidus necator* showed a direct correlation with $k_L a$, with a $171 \ \%$ increase in maximum cell concentration and a $67 \ \%$ increase in the specific growth rate when $k_L a$ increased from $183 \ to 364 \ h^{-1}$. These findings highlight the potential of the ATFR as a promising platform for gas-liquid mass transfer-limited processes, particularly in systems bioconverting poorly soluble gases such as H_2 , CH_4 , CO and O_2 .

1. Introduction

Today, the sustained accumulation of greenhouse gases (GHG) in the atmosphere, primarily carbon dioxide (CO₂) and methane (CH₄), represents one of the most important environmental, social, and technological global challenges. If this trend continues, the planet may face irreversible ecosystem disruptions, massive biodiversity loss, and severe socio-economic consequences as a result of climate change [1]. In recent years, the microbial conversion of gaseous pollutants such as CO₂ and CH₄ has emerged as a promising solution to abate GHG emissions due to the ability of microorganisms to cost-effectively transform these waste gases into value-added compounds. Microorganisms performing this process include microalgae, cyanobacteria, methanotrophs, knallgas or hydrogen-oxidizing bacteria and acetogenic species. Moreover, other organisms, such as *Escherichia coli* and yeast strains, have been genetically engineered to enable similar functionality [2].

Cupriavidus necator is a facultatively autotrophic bacterium from the knallgas group, which has shown great potential for producing fermentation-based chemicals using CO₂ as its sole carbon source. C. necator can fix CO₂ via the Calvin–Benson–Bassham (CBB) cycle, which involves three key steps: carboxylation, reduction, and regeneration. During this process, CO₂ is combined with ribulose-1,5-

bisphosphate (RuBP), reduced to glyceraldehyde-3-phosphate (G3P), and RuBP is regenerated, enabling the synthesis of sugars and other commercial organic compounds [3]. This autotrophic metabolism uses hydrogen (H2) as the electron donor and oxygen (O2) as the terminal electron acceptor. This entails safety risks when the O2 concentration falls between the lower and upper explosive limits of H2/O2/CO2 mixtures (LEL and UEL, respectively), which are approximately 6.7 % and 20 % by volume of O2, respectively [4]. During autotrophic CO2 bioconversion, CO_2 , H_2 and O_2 must first dissolve into the liquid phase to enable microbial uptake and metabolism. The massive solubilization of H₂ and O₂ requires an intensive energy input, typically provided by mechanical agitation in stirred-tank bioreactors or by local energy gradients generated by the kinetic energy of the injected fluids in nonstirred systems [5]. Due to their low solubility, H2 and O2 gas-liquid mass transfer represents a significant bottleneck in CO2 bioconversion processes [6].

The configuration and operation of gas-phase bioreactors determine the cost-effectiveness of gas-liquid mass transfer in gas fermentation processes [7]. A common strategy to overcome the limitations associated with gas solubility is to increase the volumetric mass transfer coefficient ($k_L a$) to compensate for the low concentration gradients. In this context, multiple innovative bioreactor designs have been developed

^{*} Corresponding author at: Department of Chemical and Environmental Engineering, University of Valladolid, Dr. Mergelina, s/n, 47011 Valladolid, Spain. E-mail address: raul.munoz.torre@uva.es (R. Muñoz).

and tested in various gas-phase bioprocesses with encouraging improvements in gas-liquid mass transfer efficiency. One such design is the airlift bioreactor, which offers multiple operational advantages, including prolonged gas-liquid contact time, low maintenance cost, reduced energy requirements, low shear stress on cells, and high mixing efficiency [8]. Several airlift configurations have been proposed, with the concentric-tube internal loop airlift being one of the most widely used. It consists of two concentric tubes, where the gas is introduced into the inner tube (riser), reducing the liquid density and generating a driving force that causes the liquid to descend through the outer tube (downcomer) and to recirculate continuously to the riser. Similarly, capillary Taylor flow bioreactors have recently emerged as a promising gas-phase bioreactor configuration to support the bioconversion and biodegradation of hydrophobic gaseous substrates [9-13]. These systems consist of multi-capillary channels where, depending on the gas-toliquid velocity ratio, alternating sequences of gas bubbles and liquid slugs are formed and move upward co-currently. This flow pattern-segmented, slug, or Taylor flow-enhances gas-liquid mass transfer due to the internal recirculation within the liquid and gas segments, increased interfacial area, and reduced diffusion distances [13]. However, the need for high liquid recirculation rates to maintain Taylor flow can limit the cost effectiveness of this innovative high-performance bioreactor configuration, indicating that improvements in design and operation remain an open area for investigation.

To enable the industrial-scale deployment of CO_2 and H_2 bioconversion processes, it is essential to develop reactor technologies capable of efficiently transferring poorly soluble gases—such as hydrogen—without significantly increasing the system's energy consumption. In this context, a novel Airlift Taylor Flow Reactor (ATFR) was designed, constructed, characterized and evaluated in terms of CO_2 -bioconversion performance. This configuration combines the low-cost density-driven liquid recirculation characteristic of airlift systems with the high gasliquid mass transfer of Taylor flow systems. The fluid dynamics and k_L a of the ATFR were systematically characterized with and without an external centrifugal pump-based liquid recirculation. Finally, the potential of the ATFR for H_2 -assisted CO_2 bioconversion by C. necator was assessed at different knallgas compositions and k_L a values.

2. Materials and methods

2.1. Microorganism and culture medium

A strain of *Cupriavidus necator* H16 (DSM 416), obtained from DSMZ (Germany), was used in the biotic experiments. The strain was stored in cryovials containing glycerol. Activation was carried out at 30 $^{\circ}\text{C}$ in Luria–Bertani (LB) medium composed of (g L $^{-1}$): 10 peptone, 10 NaCl, and 5 yeast extract. Following activation, the culture was transferred to a modified mineral salt medium (MSM) based on DSMZ Medium No. 81, excluding NaVO_3 and vitamins. The resulting composition was (g L $^{-1}$): 2.3 KH₂PO₄, 4.4 Na₂HPO₄·7H₂O, 1 (NH₄)₂SO₄, 0.5 MgSO₄·7H₂O, 0.01 CaCl₂·2H₂O, 0.005 MnCl₂·4H₂O, 0.05 ferric ammonium citrate, 0.5 NaHCO₃, and 5 mL of trace element solution. The trace element solution SL-6 contained (g L $^{-1}$): 0.1 ZnSO₄·7H₂O, 0.03 MnCl₂·4H₂O, 0.3 H₃BO₃, 0.2 CoCl₂·6H₂O, 0.01 CuCl₂·2H₂O, 0.02 NiCl₂·6H₂O, and 0.03 Na₂MoO₄·2H₂O.

Glass bottles (2.1 L) with rubber stoppers and aluminium screw caps, each containing 300 mL of culture medium, were sterilized at 121 °C for 20 min. Afterwards, 30 mL of fresh $\it C.$ necator inoculum and fructose (as a carbon source) at a final concentration of 10 g L $^{-1}$ were added. Cultivation was carried out using a magnetic stirring plate (Thermo, Cimarec i multipoint) at 320 rpm and 30 °C for 5 days. Following incubation, the culture was centrifuged at 13,000 rpm for 10 min. The resulting cell pellet was washed twice with distilled water to remove the residual fructose from the culture medium. Finally, the pellet was resuspended in 1 L of sterile MSM and used as the inoculum in the biotic ATFR experiments.

2.2. Airlift Taylor Flow Reactor set-up

A concentric-type airlift reactor was constructed, with the cylindrical riser (5 cm diameter × 1.5 m length) containing 97 glass capillary tubes, each with an internal diameter of 2.4 mm and a length of 1.5 m (Fig. 1B). A summary of the main geometric details of the reactor is shown in Table 1. The reactor was built using transparent polyvinyl chloride (PVC), glass, and stainless-steel modules (Fig. 1A). A packed bed of K1 Kaldnes rings (~300 mL) was placed at the gas inlet to improve air bubble disruption and a homogeneous distribution of the air bubbles entering the capillaries [11] (Fig. 1C). The total liquid volume in the reactor was 13 L. A centrifugal pump (Espa, Prisma 25, Spain) was installed to evaluate the effect of external mechanical liquid recirculation on the downcomer flow velocity and k_La. The liquid recirculated by the pump was measured using a rotameter (MRF, I). In both configurations—with and without pump-assisted—the same liquid was continuously recirculated between the riser and the downcomer, without any additional fresh water or medium feed during operation. The system was equipped with a compressor (ABAC, LT50) to inject filtered ambient air at the base of the reactor. The gas flow was measured with a rotameter (Aalborg, P Series). Fig. 1D shows a schematic diagram of the experimental set-up.

2.3. Influence of the gas flow rate and external liquid recirculation on the downcomer liquid recirculation flow rate

A coloured tracer method was used to determine the liquid recirculation flow rate in the downcomer [14,15]. This method involves injecting a tracer into the reactor and measuring the time needed to stain a specific length of the riser or downcomer. For this purpose, 13 L of distilled water and 20 mL of a 1 g L $^{-1}$ phenolphthalein solution were added to the reactor. Subsequently, 20 mL of an 8 M NaOH solution was injected at the bottom of the reactor. Afterwards, 20 mL of an 8 M HCl solution was injected to neutralise the mixture, returning it to a colourless state for a duplicate measurement under similar conditions. Videos (4 K, 60 fps) were recorded to capture the staining of the liquid in the downcomer, and video analysis was carried out using the free, opensource software Shotcut v24.06.

To ensure accuracy in the velocity determination, a metric ruler was mounted on the front side of the reactor (visible from the camera) to measure the distance travelled by the dyed fluid. The tracer, injected at the reactor's base, ascended through the riser and then descended through the downcomer. Liquid velocity was estimated by tracking the vertical displacement of a dyed pixel in the downflow, 20 cm below the downcomer inlet. This position was selected to capture a visually homogeneous and representative region, minimizing interferences caused by turbulence at the riser outlet and downcomer inlet. Each pixel was tracked for 10 s to ensure a stable measurement. This procedure was repeated for six randomly selected pixels, yielding six individual velocity measurements. The average of these values was reported as the final velocity, and the standard deviation was used as the error estimate.

It is important to note that this evaluation only considered the front-facing section of the reactor (as seen by the camera), ignoring the curvature of the downcomer, and therefore may not detect potential radial variations in the velocity profile. The camera was positioned 50 cm from the downcomer and oriented perpendicularly to its front plane.

Finally, the liquid loop flow was calculated using the annular cross-sectional area of the downcomer and the average liquid velocity at gas flow rates of 10, 20, 30, 40, 50, and 60 L $\rm min^{-1}$, and at external liquid recirculation rates of 0, 5, and 6.7 L $\rm min^{-1}$.

2.4. Influence of the gas flow rate and external liquid recirculation on the gas-liquid mass transfer coefficients

The gas-liquid oxygen mass transfer coefficient was quantified using the sulphite oxidation method, following the protocol described by

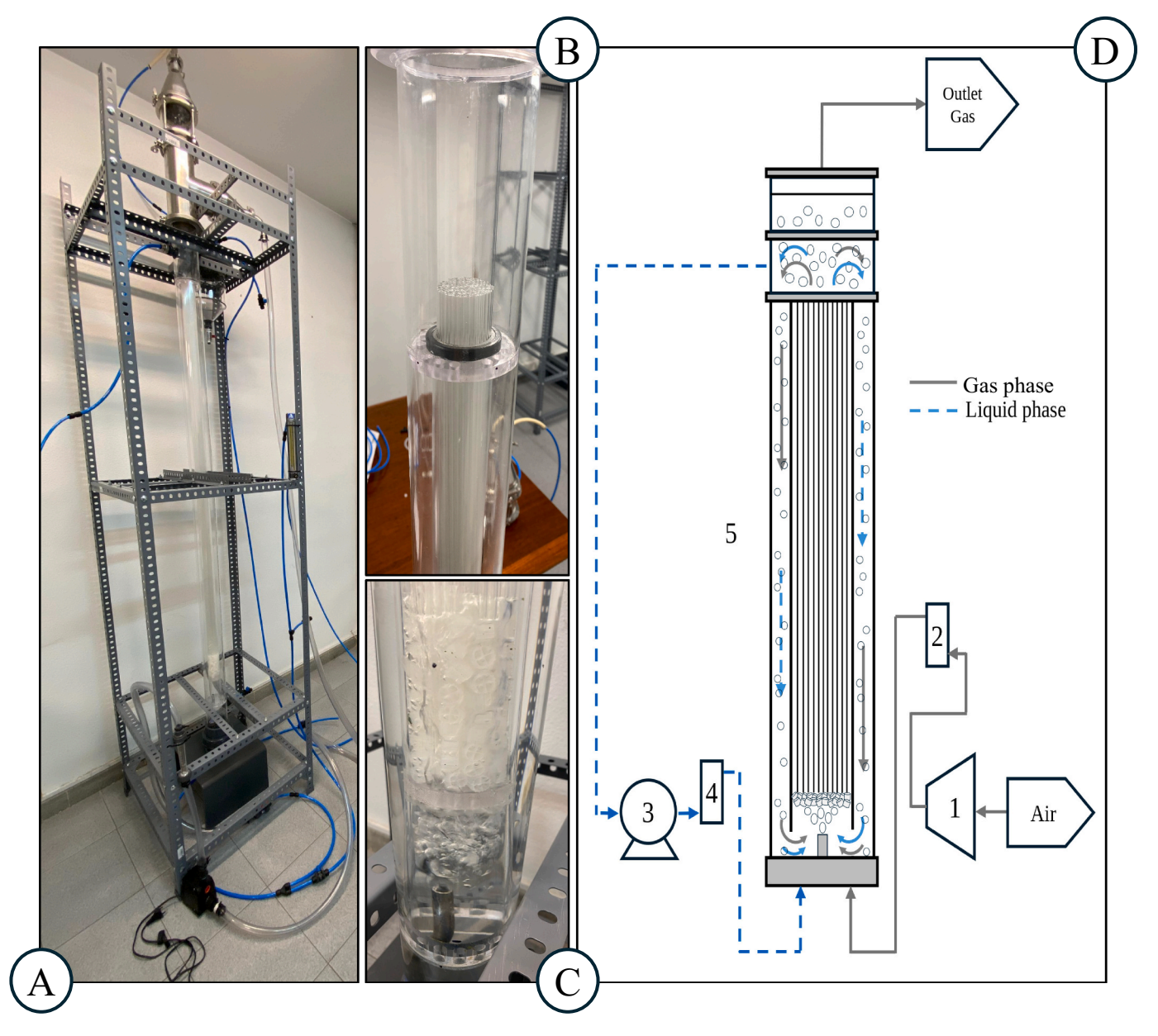


Fig. 1. Photograph of the A) ATFR, B) Capillary Riser, C) K1 Kaldnes-based gas distribution system, and D) schematic diagram of the ATFR experimental set-up (1) Compressor. (2) Rotameter. (3) Centrifugal Pump. (4) Liquid rotameter. (5) ATFR.

Table 1Main geometric characteristics of the ATFR.

Description	Value
Downcomer diameter (m)	0.9
Riser diameter (m)	0.5
Downcomer-to-riser cross-sectional area ratio	3.5
Downcomer length (m)	2.0
Capillary tubes length (m)	1.5
Number of capillary tubes	97.0
Capillaries inner diameter (m)	0.024
Working volume (m3)	0.013
Height of gas-free liquid (m)	2.2

Muñoz et al. [16]. This method allows the oxygen transfer rate (OTR, g $L^{-1}\ h^{-1})$ estimation via a Co $^{2+}$ -catalysed reaction between oxygen and sulphite at the gas-liquid interface. This reaction keeps the dissolved O_2 concentration in the liquid phase near zero. The following equation represents the oxygen mass transfer from the gas to the liquid phase:

$$OTR = \frac{dC_{O_2}}{dt} = k_L \alpha \left(C_{O_2}^* - C_{O_2} \right)$$
 (1)

Where $C_{O_2}^*$ is the O_2 saturation concentration (g L⁻¹) and C_{O_2} is the oxygen concentration (g L⁻¹) at time t (h). From the reaction's stoichiometry, the total mass of O_2 transferred to the liquid is calculated, and when normalized by the sample volume, the oxygen concentration in the liquid C_{O_2} is obtained. Plotting C_{O_2} against time yields a linear relationship, the slope of which corresponds to the OTR. Finally, the volumetric mass transfer coefficient (k_La, h⁻¹) is calculated by dividing the OTR by $C_{O_2}^*$. The k_La was determined at air flow rates of 10, 30, and 60 L min⁻¹ and for external liquid recirculation rates of 0 and 5 L min⁻¹. Each measurement was performed in duplicate.

2.5. Power consumption in the ATFR configurations

In an airlift reactor, the movement of the liquid phase is primarily

driven by the energy released during the isothermal expansion of the injected gas, from the pressure at the reactor base to the headspace pressure. Accordingly, the specific power consumption (P/V, W m $^{-3}$) of the ATFR system without forced liquid recirculation was determined using the following Eqs. [17]:

$$\frac{P}{V} = \frac{\rho_L g U_g}{1 + \frac{A_d}{A_L}} \tag{2}$$

where ρ_L is the liquid density (g L^{-1}), g is the gravitational acceleration (m s⁻²), Ad and Ar are the cross-sectional areas of the downcomer and riser (m²), respectively. The riser area was calculated as the total cross-sectional area of all capillaries, i.e., the area of a single capillary multiplied by the number of capillary tubes. The superficial gas velocity Ug (m s⁻¹) was calculated using the expression:

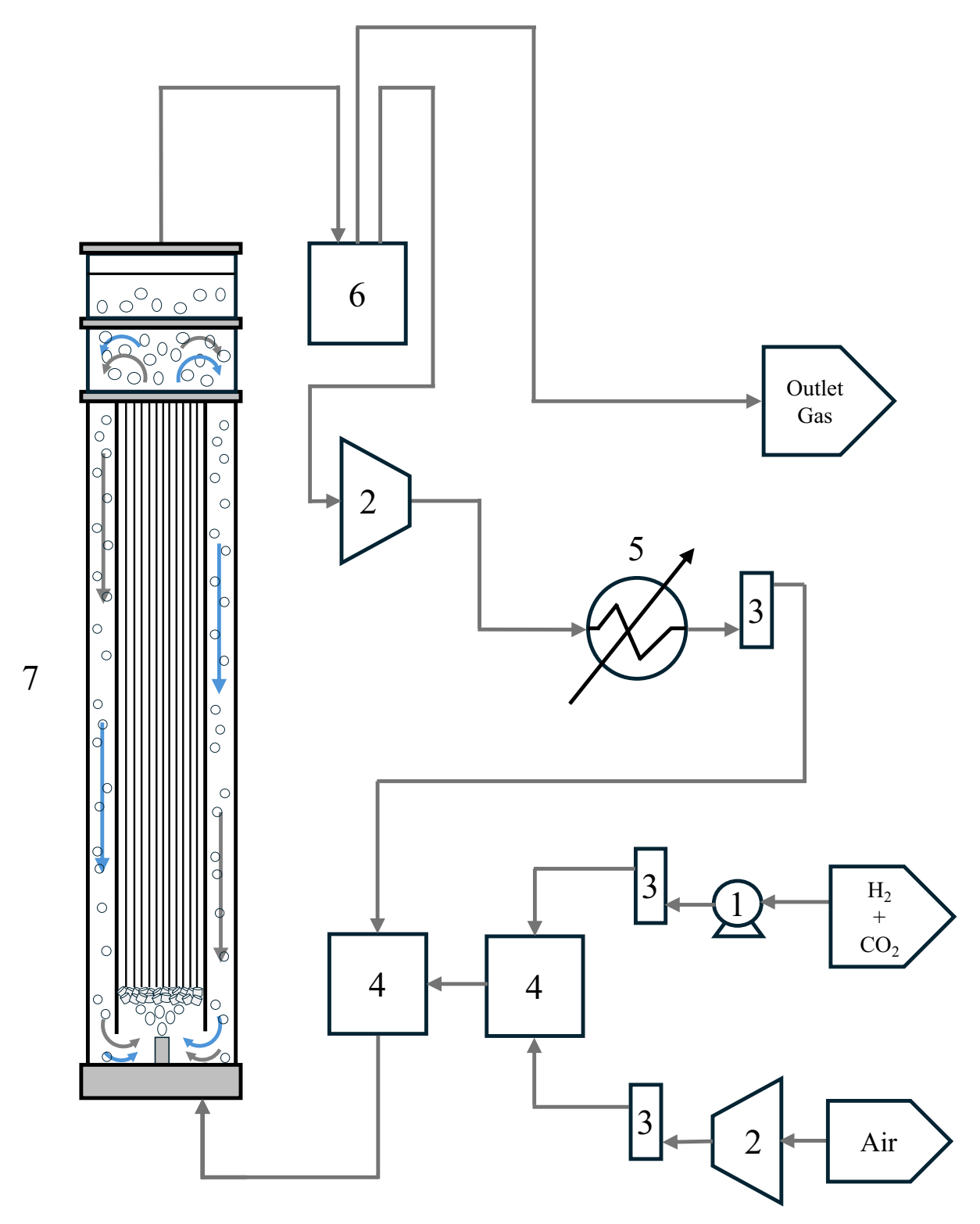


Fig. 2. Experimental system set-up (1) Peristaltic pump, (2) Compressor, (3) Rotameter, (4) Gas mixing chamber, (5) Condenser, (6) Water trap, (7) ATFR.

$$U_g = \frac{Q_m RT}{h_L A_r \rho_L g} \ln \left(1 + \frac{\rho_L g h_L}{P_h} \right)$$
(3)

where Q_m is the molar gas flow rate (mol s⁻¹), R is the universal gas constant (J mol⁻¹ K⁻¹), T is the absolute temperature of the gas phase (K), h_L is the static height of the gas-free liquid (m), and P_h is the headspace pressure (Pa).

In contrast, for the ATFR operated with external pump-assisted liquid recirculation, the power input calculated from Eq. (2) –representing the contribution from isothermal gas expansion—was complemented by the kinetic energy of the liquid entering the reactor, following the approach proposed by Fadavi and Chisti [18]:

$$\frac{P}{V} = \frac{\rho_L g U_g}{1 + \frac{A_d}{A}} + \frac{Q_L}{2V_L} \rho_L v_{LN}^2 \tag{4}$$

where Q_L is the volumetric liquid flow rate $(m^3\ h^{-1})$, V_L is the liquid volume in the reactor (m^3) , and v_{LN} is the velocity of the liquid at the reactor inlet $(m\ s^{-1})$. The second and fourth terms from the original equation proposed by Fadavi and Chisti—corresponding to the kinetic energy of gas injection and the energy loss in the sparger zone—were not considered in this estimation, as the ATFR configuration employed in this study does not include a sparger system. Therefore, in this case, the energy contribution from gas and liquid injection is negligible compared to the two retained terms.

2.6. Assessment of the autotrophic growth of Cupriavidus necator in ATFR

Batch cultures of *Cupriavidus necator* were conducted to evaluate the effect of the volumetric mass transfer coefficient on cell growth. For this purpose, a compressor (Thomas, 910CDC22) was integrated into the ATFR system to enable internal gas recirculation. A peristaltic pump (Watson Marlow, 120 U) was used to supply a gaseous mixture with a composition of 20 % $\rm CO_2$ and 80 % $\rm H_2$ (v/v, 1 atm), which was stored in a 100 L Tedlar bag, while an air compressor (PUSKA, Spain) was used to adjust the knallgas composition. The ATFR was jacketed to maintain the cultivation broth at 30 °C via recirculation of hot water from a DIGITHERM 200 thermostatic bath (SELECTA, Spain). The complete experimental set-up is shown in Fig. 2.

The filtered fresh air feed was mixed with the CO₂ and H₂ stream in a gas mixing chamber to obtain a final volumetric composition of 16 %:59 %:5 %:20 % (CO₂:H₂:O₂:N₂). This composition was selected as a safety measure to ensure system operation below the LEL [4]. Additional experiments were performed using a composition above the UEL, more specifically 2 %:5 %:20 %:73 % (CO₂:H₂:O₂:N₂). The resulting gas stream was combined with the recirculating gas flow in a second chamber before entering the ATFR from the bottom. The gas flowed upward through the capillaries in the riser and exited from the top of the reactor, entering a third chamber that functioned as a water trap, where entrained liquid was collected. Inside this trap, the gas stream was split into the recirculation and exhaust gas streams. The gas compressor then propelled the recirculating gas through a condenser maintained at 10 °C to remove any remaining moisture. The flow rates of the air supply, the CO₂:H₂ mixture, and the gas recirculation loop were controlled using rotameters (Aalborg, P Series). Duplicate experiments were performed for each gas composition, varying the gas recirculation from 3 to 10 L min⁻¹. The dissolved oxygen concentration (DO), temperature, pH and optical density (OD) in the cultivation broth, and the concentrations of CO2, H2, O2, and N2 in inlet and outlet gas streams were monitored twice a day.

2.7. Analytical procedures

DO and temperature were measured using an Oxi 3310 oximeter (WTW, Germany), while the pH was monitored with a SensION $^{\rm TM}+PH3$

pH meter (HACH, Spain). Optical density was measured at 600 nm using a UV-2550 spectrophotometer (Shimadzu, Japan). Gas concentrations were determined by gas chromatography with thermal conductivity detection (GC-TCD) using an Agilent 8860 system (California, USA), following the procedure described by Regueira-Marcos et al. [19].

3. Results and discussion

3.1. Influence of the gas flow rate and external liquid recirculation on the downcomer liquid recirculation flow rate

The use of an external centrifugal pump to improve liquid recirculation in the system was evaluated. Fig. 3 shows the liquid velocities measured in the downcomer under pump-assisted and non-assisted conditions. Significantly lower liquid velocities were observed in the downcomer of the ATFR with internal recirculation flow rates of 5 and $6.7~L~min^{-1}$ compared to the system without forced recirculation (0 L min⁻¹). In fact, the liquid velocity in the downcomer decreased at increasing external liquid recirculation flow rates mediated by the centrifugal pump, regardless of the air flow rate tested. For instance, the maximum velocity recorded in the downcomer was 7.2 \pm 0.5 cm \mbox{s}^{-1} at an air flow rate of 60 L min⁻¹ without external liquid recirculation. This velocity decreased to 2.5 \pm 0.2 cm s^{-1} at a liquid recirculation rate of 5 L min $^{-1}$ and to 0.6 \pm 0.2 cm s $^{-1}$ at a recirculation flow of 6.7 L min $^{-1}$ under the same air flow rate of 60 L min⁻¹. In airlift reactors, the driving force for liquid movement is generated by the difference in gas hold-up between the riser and the downcomer. This gas hold-up changes fluid density, resulting in liquid recirculation [20]. The hydrodynamics in airlift reactors are altered when a pump is used for external liquid recirculation, since the suction generated by the pump reduces the gas hold-up between the riser and the downcomer. Hence, the hydrostatic pressure gradient caused by the density difference is reduced as gas hold-up decreases, which negatively influences the liquid velocity in the downcomer [21]. Interestingly, the decrease in the liquid velocity in the downcomer at external liquid recirculation of 5 and 6.7 L min⁻¹ occurred to a larger extent at increasing gas flow rates. For instance, the liquid velocity in the downcomer at a gas flow rate of 10 L min⁻¹ decreased by 57.1 and 76.2 % at external liquid recirculation of 5 and 6.7 L min⁻¹, respectively, and by 65.3 and 95.8 % at a gas flow rate of 60 L min^{-1} .

On the other hand, the liquid velocity in the downcomer increased linearly as the inlet gas flow rate increased in the absence of external liquid recirculation. This behaviour was attributed to the lower gas holdup and to the increased influence of wall friction at low gas flow rates,

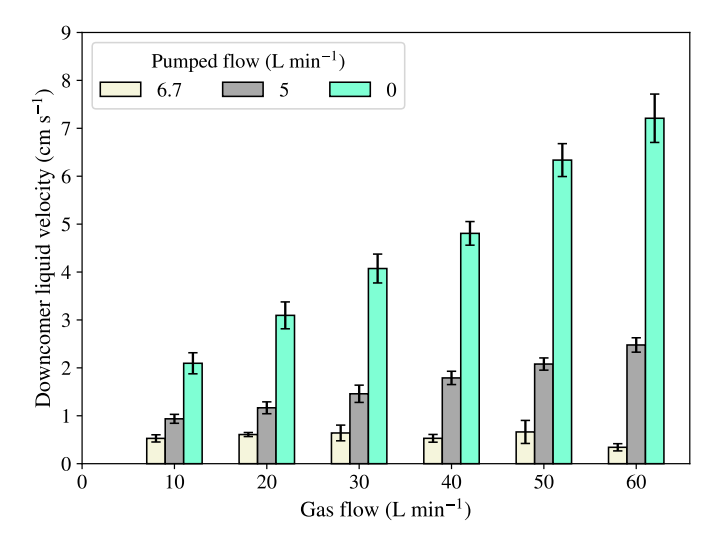


Fig. 3. Liquid velocity in the downcomer as a function of the external pump-driven recirculation flow rate at increasing gas flow rates.

which slows down the liquid movement. At higher gas flow rates, the gas hold-up increases and the liquid becomes more turbulent, significantly reducing the influence of wall friction [15]. Additionally, the number of gas bubbles retained between the riser and the downcomer increases, enhancing the system's driving force due to a greater density difference between the two regions.

The volumetric flow rate of descending liquid ($Q_{L,d}$, L min⁻¹) was calculated using eq. (5) based on the measured liquid velocity in the downcomer:

$$Q_{L,d} = \nu_{L,d} \bullet A_d \bullet 0.06 \tag{5}$$

Where $v_{L,d}$ is the liquid velocity in the downcomer (cm s⁻¹), A_d is the annular cross-sectional area of the reactor corresponding to the downcomer (cm²) and 0.06 is the unit conversion factor.

The liquid recirculation flow rate shown in Fig. 4 corresponds to the sum of the liquid recirculated through the downcomer and the external pump-assisted recirculation. At an external liquid flow rate of 6.7 L min⁻¹, the liquid recirculated through the downcomer accounted for an average of 14.5 \pm 2.7 % of the total recirculated flow within the entire gas flow range tested. Similarly, when the pump flow rate was reduced to 5 L min $^{-1}$, an average of 41.9 \pm 7.0 % of the total flow was obtained through the downcomer. Interestingly, only at gas flow rates below 30 L min⁻¹ the total liquid recirculation flow was higher when external liquid recirculation was implemented. At 30 L min⁻¹ of gas flow rate, the total liquid flow was equivalent with and without external pump-assisted recirculation, while at gas flow rates above 30 L min⁻¹ the system without external liquid recirculation achieved higher total liquid flow rates, reaching a maximum value of $14.9 \pm 1.0 \, \mathrm{L \, min^{-1}}$. This represents a maximum increase of 47 % in the recirculating liquid flow when no pump is used.

3.2. Influence of the gas flow rate and external liquid recirculation on the gas-liquid mass transfer coefficients

A direct linear relationship between the gas flow rate and k_La values was observed, indicating that higher gas flow rates significantly enhance the oxygen gas-liquid transfer (Fig. 5). Thus, the k_La values increased linearly from $363.5\pm0.91\ h^{-1}$ at a gas flow rate of $10\ L\ min^{-1}$ up to $891\pm23\ h^{-1}$ at a gas flow rate of $60\ L\ min^{-1}$. This behaviour was attributed to the increased generation of gas bubbles, intensifying turbulence within the multicapillary riser and promoting bubble fragmentation, resulting in a smaller average bubble size. The reduction in bubble size increases the gas-liquid interfacial area due to a higher surface area-to-

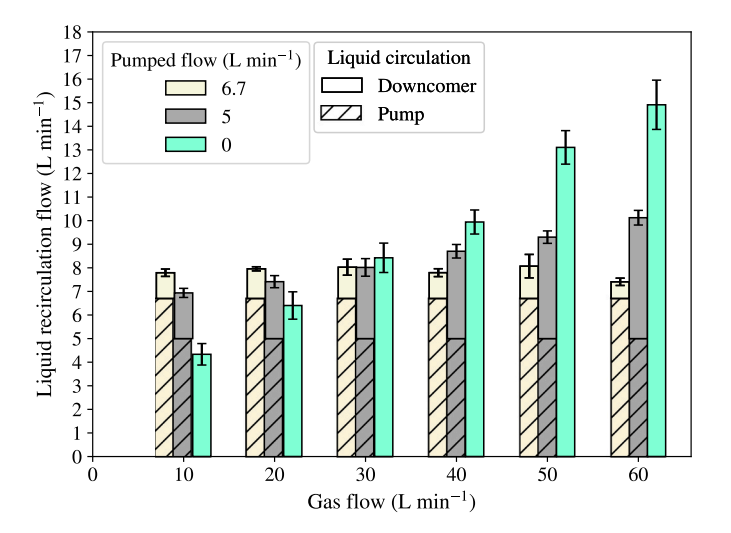


Fig. 4. Liquid recirculation flow rate in the downcomer (dotted bars) and in the external recirculation pipeline (dashed bars) at different external pump-driven recirculation flow rates at increasing gas flow rates.

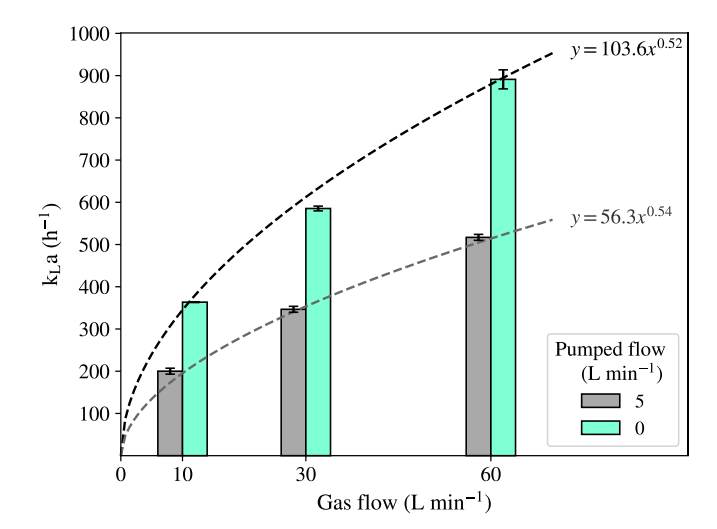


Fig. 5. Influence of the gas flow rate on the volumetric oxygen mass transfer coefficient with and without external liquid recirculation. Dashed lines represent the fitted model for each condition.

volume ratio, thereby improving mass transfer efficiency from the gas phase to the liquid phase. In addition, increasing the gas velocity induces a corresponding increase in liquid velocity, which enables efficient recirculation of bubbles entering the downcomer and facilitates their return to the riser. The presence of gas bubbles in the downcomer extends the contact time between phases, further enhancing the overall efficiency of the oxygen gas-liquid mass transfer process.

The maximum $k_L a$ value obtained was $891 \pm 23 \ h^{-1}$ at a gas flow rate of $60 \ L \ min^{-1}$, which is among the higher values reported for bioreactors without mechanical agitation. For instance, a maximum $k_L a$ of $462 \pm 12 \ h^{-1}$ at a gas flow of $9 \ L \ min^{-1}$ and a liquid flow of $6 \ L \ min^{-1}$ in a capillary reactor with a volume of $8.4 \ L$ and $25 \ capillaries$ [9]. In contrast, typical $k_L a$ values reported for airlift reactors generally do not exceed $250 \ h^{-1}$ [10,22–26]. The significant increase observed in the present ATFR compared to conventional airlift reactors can be attributed to the presence of Taylor flow in the riser. To promote segmented (Taylor) flow, surface tension must dominate over other forces such as gravity. This condition can be assessed using the Bond number (Bo), defined as the ratio of gravitational to surface tension forces:

$$Bo = \frac{\rho_L g d^2}{\gamma} \tag{6}$$

Where d is the inner diameter of the capillary tube (m) and γ the surface tension (N m⁻¹). A low Bond number indicates that surface tension dominates the flow regime, which is favourable for slug flow formation. Previous studies have proposed that a Bo value below 3.3 is required to achieve slug flow in capillary systems [27]. In the present configuration, the calculated Bo was 0.79, supporting the formation of slug-like bubbles that rise through the capillaries, enhancing mass transfer through internal liquid recirculation between bubbles and the friction generated between the bubble and the thin liquid film formed along the capillary wall [28]. On the other hand, the operation of the ATFR with an external liquid recirculation of 5 L min⁻¹ entailed maximum k_La values of 517.0 \pm 23.88 h⁻¹, approximately 75 % lower, on average, than the k_L a values achieved without forced recirculation. This reduction was attributed to the decreased gas retention in the riser, which led to a lower liquid recirculation rate. In this context, low liquid recirculation velocities in airlift reactors result in operation under the so-called bubble-free regime (Regime I) [20]. This regime is characterized by the absence or minimal presence of bubbles in the downcomer, which are not recirculated to the riser, substantially reducing the gas-liquid contact time.

Additionally, the gas hold-up directly influences the interfacial area available for gas-liquid mass transfer. Previous studies have shown that

an increase in gas hold-up typically leads to higher k_I a values due to enhanced interfacial area and longer gas residence times in the liquid phase [29-32]. These studies emphasize the direct correlation between gas hold-up and effective interfacial area, particularly under homogeneous flow regimes where higher gas flow rates promote the formation of smaller, more uniformly distributed bubbles. This is attributed to increased nucleation and shear rates at the injection point, along with reduced coalescence, resulting in higher bubble densities and smaller mean diameters, which in turn enhance gas-liquid mass transfer [31]. In airlift bioreactors, the hydrodynamics are especially complex due to bubble breakup, coalescence, and deformation phenomena, as well as interactions between bubbles and the liquid phase [29]. In this context, the suction location for forced recirculation in the ATFR may have promoted bubble capture by the pump. The passage of the gas-liquid mixture through the pump may have triggered coalescence, increasing the average bubble diameter and thus reducing the interfacial area, partially explaining the observed decrease in k_La. Additionally, the pressure gradient imposed by the pump flow exceeded that generated naturally by the density difference between the riser and downcomer (Fig. 4), disrupting the internal circulation pattern typical of airlift systems. Finally, the increased inlet liquid velocity from the pump may have altered the flow regime within the capillary, favouring a transition from slug flow to churn, which is less encouraging for gas-liquid mass transfer [33].

Overall, the high $k_{\rm L}a$ values obtained revealed that the novel ATFR herein developed represents a promising alternative for processes requiring high gas-liquid mass transfer, particularly in the treatment or bioconversion applications involving poorly soluble gases such as hydrogen, methane, carbon monoxide and oxygen.

3.3. Energy-performance of the ATFR with and without forced liquid recirculation

Fig. 6 shows the relationship between P/V and k_La in the ATFR with and without pump-assisted recirculation, along with different configurations of airlift reactors and stirred fermenters reported in the literature. A linear increase in k_La was observed as P/V increases, since the energy consumption of the ATFR proposed in this study was primarily associated with the expansion of the fed gas. The ATFR configuration without forced liquid recirculation achieved the highest k_La values while consuming between 5 % and 1 % less energy compared to the configuration with forced liquid recirculation. This difference became less

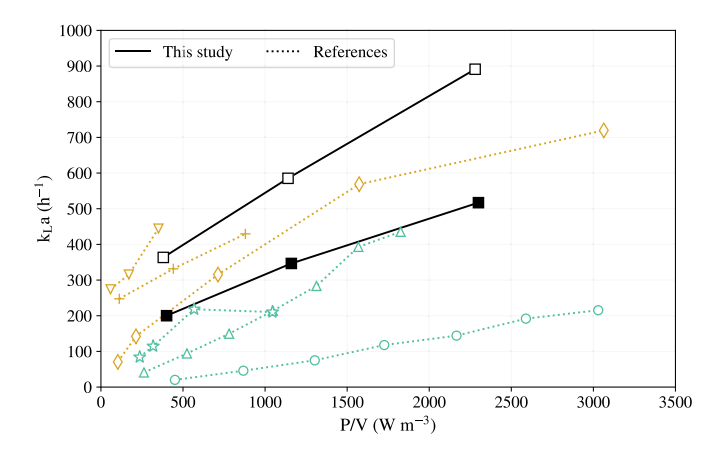


Fig. 6. $k_L a$ as a function of the power consumption in present and previous studies: (\blacksquare) ATFR with pump-assisted recirculation, (\square) ATFR without forced liquid recirculation. Yellow symbols represent stirred bioreactors: (∇) Stirred Airlift [37], (+) Stirred tank reactor [37], (+) Multiple-impeller fermenter [35]. Turquoise symbols correspond to bioreactors without mechanical agitation: (+) Airlift with forced circulation loop [18], (+) Airlift with helical plates [34], (+) Conventional Airlift [34].

pronounced at higher gas flow rates, as the kinetic energy contribution from the recirculated liquid became negligible relative to the energy derived from isothermal gas expansion. Compared with other reported systems, the ATFR achieved consistently higher k_La values for the same P/V in most cases. Thus, at a P/V of \sim 380 W m⁻³, the ATFR reached a k_La 18 times higher than that obtained in a conventional airlift reactor [34] and 1.5 times higher than in a multi-impeller stirred fermenter [35]. Similarly, the k_La achieved in the ATFR at a P/V of \sim 2280 W m⁻³ was 4.6 and 1.3 times higher, respectively, than those systems. Although stirred bioreactors have shown high k_La values—and under certain conditions comparable to the ATFR at similar power input-they are restricted by their maximum stirrer speed. Furthermore, excessive mechanical agitation can produce high shear stress, which may modify cell morphology and cause mechanical damage, ultimately leading to cell lysis or loss of viability—even in the otherwise resilient cells [36]. These effects can greatly reduce bioconversion performance. In contrast, the integration of capillaries and the establishment of Taylor flow in the ATFR riser could significantly improve the energy efficiency, as higher k_I a values were achieved at similar or lower power consumption levels compared to other bubbling systems.

These results suggest that the ATFR could represent an energy-efficient alternative for gas-liquid mass transfer compared to conventional technologies. Additionally, its agitation-free design makes it inherently safer for $\rm CO_2/H_2$ bioconversion processes, as it removes ignition risks associated with electric motors operating in explosive gas atmospheres.

3.4. Assessment of the autotrophic growth of Cupriavidus necator in ATFR

The pH of the culture broth remained constant at 6.8 ± 0.03 throughout the 9-day cultivation period in all experiments with C. necator. Process operation at 3 L min⁻¹ — which corresponded to a k_I a of 183 h⁻¹, estimated from the fitted model (Fig. 5) — with a gas mixture below the lower explosive limit (16 %, 59 %, 5 %, 20 % CO₂:H₂: O₂:N₂) resulted in a maximum cell concentration of 0.35 g_{CDW} L⁻¹ and a specific growth rate (μ) of 0.009 h⁻¹ within 7 days of operation (Fig. 7). The increase in the k_La up to 364 h^{-1} by increasing the internal gas recirculation from 3 L min⁻¹ to 10 L min⁻¹ under the same inlet gas composition resulted in a higher maximum biomass concentration of $0.95 \, g_{CDW} \, L^{-1}$ and a μ of $0.015 \, h^{-1}$ in the same cultivation period. Thus, an 99 % enhancement in kLa induced a 171.4 % increase in the maximum cell concentration and a 67 % higher specific growth rate of C. necator. However, under this operational condition, C. necator growth was still limited by dissolved oxygen availability in the cultivation broth. Indeed, the DO concentration remained constant at 0.1 mg L^{-1} under the stationary phase in assays conducted with LEL gas mixtures. In this context, Lambauer et al. [38] reported a similar maximum

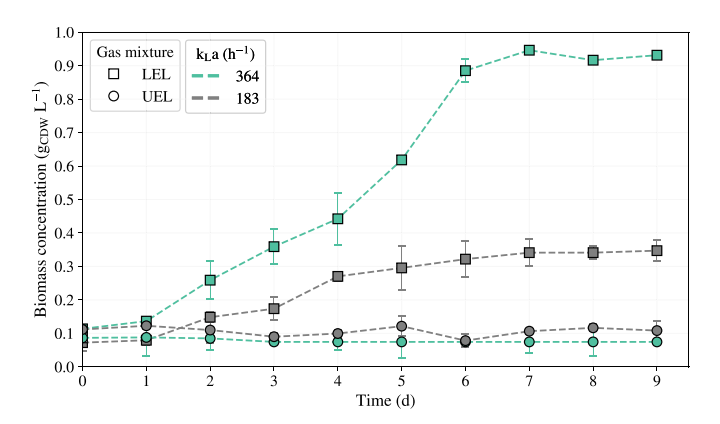


Fig. 7. Influence of the $k_{\rm L}a$ and gas mixture composition on the autotrophic growth of *Cupriavidus necator*.

concentration of *C. necator* (1.2 g_{CDW} L^{-1}) in a 1 L stirred-tank reactor operated under a constant gas flow rate (400 mL min⁻¹) with a composition of 10 %:85 %:2 % (CO_2 : H_2 : O_2) for 7 days. Thus, in a subsequent experiment, in order to overcome O_2 limitation and achieve higher biomass concentrations, the O_2 supply was gradually increased from 0.02 atm (total inlet flow rate 97 mL min⁻¹) to 0.12 atm (\sim 582 mL min⁻¹), reaching 6.5 g_{CDW} L^{-1} . Similarly, Tanaka et al. [39] reported the highest biomass concentration of *C. necator* to date (91.3 g L^{-1}) using a CO_2 , H_2 , and O_2 gas mixture with a composition of 8.3 %:85.2 %:6.3 % in a 2 L glass jar fermenter equipped with a brush motor supporting a k_L a of 2970 h^{-1} .

Cell growth was completely inhibited when the gas mixture exceeded the UEL. This phenomenon was attributed to the high oxygen content in the feed gas, which increased the DO concentration to values above 5 mg $\rm L^{-1}$. According to Tanaka et al. [39], the maximum specific growth rate of *C. necator* under autotrophic conditions was observed at a DO concentration of approximately 1.7 mg $\rm L^{-1}$. DO levels exceeding 3 mg $\rm L^{-1}$ have been associated with inhibitory effects on *C. necator* growth due to the deactivation of [NiFe]-hydrogenases involved in H₂ metabolism [40]. Moreover, a low H₂ concentration entailed a limited electron donor availability, which ultimately reduced CO₂ uptake and impaired biomass accumulation [41].

Overall, these results demonstrate that increasing k_La enhances cell growth by ensuring a sufficient O2 and H2 transfer rate, maintaining a sustained oxygen supply to the culture medium. In the ATFR validated herein, the oxygen gas-liquid mass transfer can be further improved without altering the feed flow rate or gas composition. While a maximum abiotic k_La of 891 h⁻¹ was achieved at a gas flow rate of 60 L \min^{-1} , the biotic assays were carried out at much lower flow rates (~10 and 3 L min⁻¹), resulting in k_La values of 364 h⁻¹ and 183 h⁻¹, respectively. This difference was due to operational restrictions: the fresh gas supply was limited to 0.06 L min⁻¹ to reduce hydrogen losses in the outlet gas stream, and the internal gas recirculation was limited by the system pressure drop and the available gas-tight recirculation compressor capacity, which prevented operation at higher flow rates. Overcoming this limitation would require a high-capacity compressor capable of providing $\sim\!60~L~min^{-1}$ of gas recirculation. Under these conditions, a k_La close to 900 h⁻¹—already achieved in abiotic characterization—could then be replicated under biotic conditions. According to previous studies, the optimal gas composition for autotrophic C. necator cultures is 10 % CO₂, 70 % H₂ and 20 % O₂ [40]. However, this composition exceeds the lower explosive limit of O₂ in hydrogen mixtures (6.9 % ν/ν), making its use unsafe under conventional laboratory conditions. For this reason, most studies operate with O2 concentrations below this threshold to avoid ignition risks due to the extremely low minimum ignition energy. While some laboratories have adopted explosion-proof equipment and safety infrastructure, gas extraction systems, and anti-static flooring [38], the implementation of such safety measures typically requires substantial investment. The ATFR, by providing significantly enhanced mass transfer rates, offers an alternative approach to ensure sufficient dissolved oxygen levels without requiring explosive gas compositions, thereby enabling safe operation while sustaining high microbial growth.

3.5. Maintenance and cleaning requirements for the ATFR

Biomass accumulation can compromise the hydrodynamic stability and operational performance of bioreactors, particularly in capillary systems, where small internal diameters are employed. Biomass or salt blockages or deposits inside the tubes may lead to a decline in reactor performance. During the 9-day biotic experiments conducted in this study, no signs of clogging or visible biomass accumulation were observed inside the capillaries. This observation is consistent with previous studies reporting that, in capillary systems, the high shear forces generated within the tubes can inhibit cell adhesion and prevent biofilm formation [42]. This was also observed by Kraakman and co-workers

[9,42], who conducted continuous cultures lasting 100 and 150 days, respectively, in bioreactors equipped with 25 glass capillary conduits (internal diameter of 2.4 mm), and reported no biomass accumulation or attachment in any of the channels.

Nonetheless, for the continuous operation and potential scale-up of the ATFR, it might be necessary to implement preventive cleaning and maintenance strategies. In biotechnological systems, effective clean-in-place (CIP) and backflushing protocols have been developed, enabling the removal of deposits without the need to dismantle the reactor, while optimizing water, chemical, and energy consumption [43,44]. Integrating such cleaning routines will be essential to ensure the long-term operational viability of the ATFR, where the progressive accumulation of organic and inorganic residues could alter flow distribution, increase pressure drop, and compromise gas-liquid mass transfer performance.

4. Conclusions

This study engineered, for the first time, an innovative bioreactor that combines the cost-effectiveness of airlift systems with the high-mass transfer potential of capillary Taylor flow reactors. The implementation of external mechanical liquid recirculation negatively modified the system's hydrodynamics by decreasing the liquid velocity in the downcomer, thereby reducing both the total liquid recirculation and the $k_{L}a$ value. The multicapillary structure of the riser enabled the system to achieve high mass transfer rates compared to conventional airlift reactors, reaching a maximum $k_{L}a$ of $891\pm23\,h^{-1}$ without external forced recirculation. The autotrophic growth of *C. necator* improved significantly when increasing $k_{L}a$. These findings demonstrate the potential of ATFRs with internal gas recirculation as a robust alternative for overcoming gas-liquid mass transfer limitations in bioprocesses.

However, CO_2 and H_2 bioconversion processes present important safety and scalability challenges that must be addressed in future studies to enable the safe and efficient scale-up of technologies such as the ATFR. While this study was conducted under controlled laboratory conditions, future implementations should incorporate explosion-proof components, gas detection systems, appropriate ventilation, and recirculation circuits designed to prevent hazardous O_2 accumulation—particularly when operating at high gas flow rates to maximize mass transfer. These considerations will be essential to realize the industrial potential of the ATFR system fully.

CRediT authorship contribution statement

Pedro Cruz: Writing – original draft, Visualization, Validation, Methodology, Investigation, Formal analysis, Conceptualization. Raquel Lebrero: Writing – review & editing, Supervision, Funding acquisition. Alberto Vergara-Fernández: Writing – review & editing, Supervision. Raúl Muñoz: Writing – review & editing, Supervision, Resources, Project administration, Funding acquisition, Conceptualization.

Declaration of competing interest

The authors declare that they have no known competing financial interests or personal relationships that could have appeared to influence the work reported in this paper.

Acknowledgments

The Spanish Research Agency is gratefully acknowledged for the financial support to conduct this research (PDC2022–133394-I00). This research was also funded by the Chilean National Agency for Research and Development (ANID) through the following projects: National PhD Scholarship Folio 21220445, Doctoral Cotutele Folio 21220445, Anillo ATE220045, and Fondecyt 1240411. The authors also acknowledge Laura Vargas-Estrada for providing training in analytical methods and

biological procedures, and Andrés Felipe Torres Franco for his contribution to the discussion on reactor construction and interpretation of results.

Data availability

Data will be made available on request.

References

- [1] Z. Liu, K. Wang, Y. Chen, T. Tan, J. Nielsen, Third-generation biorefineries as the means to produce fuels and chemicals from CO2, Nat. Catal. 3 (2020) 274–288, https://doi.org/10.1038/s41929-019-0421-5.
- [2] R. Tang, X. Yuan, J. Yang, Problems and corresponding strategies for converting CO2 into value-added products in Cupriavidus necator H16 cell factories, Biotechnol. Adv. 67 (2023) 108183, https://doi.org/10.1016/j. biotechadv.2023.108183.
- [3] C. Durall, P. Lindblad, Mechanisms of carbon fixation and engineering for increased carbon fixation in cyanobacteria, Algal Res. 11 (2015) 263–270, https:// doi.org/10.1016/j.algal.2015.07.002.
- [4] Y. Miyahara, C.-T. Wang, M. Ishii-Hyakutake, T. Tsuge, Continuous Supply of Non-Combustible Gas Mixture for Safe Autotrophic Culture to Produce Polyhydroxyalkanoate by Hydrogen-Oxidizing Bacteria, Bioengineering 9 (2022) 586, https://doi.org/10.3390/bioengineering9100586.
- [5] M. Śmiechowski, Molecular hydrogen solvated in water a computational study,
 J. Chem. Phys. 143 (2015) 244505, https://doi.org/10.1063/1.4938571.
- [6] B. Geinitz, A. Hüser, M. Mann, J. Büchs, Gas fermentation expands the scope of a process network for material conversion, Chem. Ing. Tech. 92 (2020) 1665–1679, https://doi.org/10.1002/cite.202000086.
- [7] K.A. Stone, M.V. Hilliard, Q.P. He, J. Wang, A mini review on bioreactor configurations and gas transfer enhancements for biochemical methane conversion, Biochem. Eng. J. 128 (2017) 83–92, https://doi.org/10.1016/j. bej.2017.09.003.
- [8] J. Saleh-Cumsille, P. Cruz, C. Huiliñir, F. Scott, A. Vergara-Fernández, A new methodology to determine kL a in airlift reactors based on a non-intrusive image analysis technique, J of Chemical Tech & Emp; Biotech (2025) jctb.7836, https://doi.org/10.1002/jctb.7836.
- [9] N.J.R. Kraakman, J. González-Martín, C. Pérez, E. Rodríguez, R. Lebrero, M. A. Deshusses, R. Muñoz, Hydrophobic air pollutants removal at one second gas contact in a multi-channel capillary bioreactor, J. Environ. Chem. Eng. 11 (2023) 110502, https://doi.org/10.1016/j.jece.2023.110502.
- [10] J. Rocha-Rios, G. Quijano, F. Thalasso, S. Revah, R. Muñoz, Methane biodegradation in a two-phase partition internal loop airlift reactor with gas recirculation, J. Chem. Technol. Biotechnol. 86 (2011) 353–360, https://doi.org/ 10.1002/jctb.2523.
- [11] R. Herrero-Lobo, A.F. Torres Franco, R. Lebrero, M.D.R. Rodero, R. Muñoz, Evaluation of the influence of the gas residence time and biomass concentration on methane bioconversion to ectoines in a novel Taylor flow bioreactor, J. Environ. Manag. 373 (2025) 123592, https://doi.org/10.1016/j.jenvman.2024.123592.
- [12] R. Herrero-Lobo, A.F. Torres Franco, W.M. Llamas-Ramos, V. Monsalvo, P. Zamora, F. Rogalla, R. Lebrero, M.D.R. Rodero, R. Muñoz, Influence of design and operational parameters of a Taylor flow reactor on the bioconversion of methane to ectoines, Journal of Environmental Chem. Eng 12 (2024) 114323, https://doi.org/10.1016/j.jece.2024.114323.
- [13] C.R. Cattaneo, Y. Rodríguez, E.R. Rene, O. García-Depraect, R. Muñoz, Biogas bioconversion into poly(3-hydroxybutyrate) by a mixed microbial culture in a novel Taylor flow bioreactor, Waste Manag. 150 (2022) 364–372, https://doi.org/ 10.1016/j.wasman.2022.07.017.
- [14] T. Vorapongsathorn, P. Wongsuchoto, P. Pavasant, Performance of airlift contactors with baffles, Chem. Eng. J. 84 (2001) 551–556, https://doi.org/ 10.1016/S1385-8947(00)00385-5.
- [15] P. Wongsuchoto, P. Pavasant, Internal liquid circulation in annulus sparged internal loop airlift contactors, Chem. Eng. J. 100 (2004) 1–9, https://doi.org/ 10.1016/j.cej.2003.11.003.
- [16] R. Muñoz, C. Soto, C. Zuñiga, S. Revah, A systematic comparison of two empirical gas-liquid mass transfer determination methodologies to characterize methane biodegradation in stirred tank bioreactors, J. Environ. Manag. 217 (2018) 247–252, https://doi.org/10.1016/j.jenvman.2018.03.097.
- [17] B. Guieysse, G. Quijano, R. Muñoz, Airlift Bioreactors, in: Comprehensive Biotechnology, Elsevier, 2011, pp. 199–212, https://doi.org/10.1016/B978-0-08-088504-9.00095-7.
- [18] A. Fadavi, Y. Chisti, Gas-liquid mass transfer in a novel forced circulation loop reactor, Chem. Eng. J. 112 (2005) 73–80, https://doi.org/10.1016/j. cej.2005.06.009.
- [19] L. Regueira-Marcos, O. García-Depraect, R. Muñoz, Continuous two-stage lactate-driven dark fermentation process for enhanced biohydrogen production from food waste, J Water Process Eng 67 (2024) 106116, https://doi.org/10.1016/j.jwpe.2024.106116.
- [20] L. Li, X. Xu, W. Wang, R. Lau, C.-H. Wang, Hydrodynamics and mass transfer of concentric-tube internal loop airlift reactors: A review, Bioresour. Technol. 359 (2022) 127451, https://doi.org/10.1016/j.biortech.2022.127451.

- [21] X. Xu, Y. Zhang, Hydrodynamics and mass transfer in an airlift loop reactor: comparison between using two kinds of spargers, Processes 12 (2023) 35, https://doi.org/10.3390/pr12010035.
- [22] M. Juraščík, M. Blažej, J. Annus, J. Markoš, Experimental measurements of volumetric mass transfer coefficient by the dynamic pressure-step method in internal loop airlift reactors of different scale, Chem. Eng. J. 125 (2006) 81–87, https://doi.org/10.1016/j.cej.2006.08.013.
- [23] Y. Chisti, U.J. Jauregui-Haza, Oxygen transfer and mixing in mechanically agitated airlift bioreactors, Biochem. Eng. J. 10 (2002) 143–153, https://doi.org/10.1016/ \$1369-703X(01)00174-7.
- [24] K. Mohanty, D. Das, M.N. Biswas, Mass transfer characteristics of a novel multistage external loop airlift reactor, Chem. Eng. J. 133 (2007) 257–264, https://doi. org/10.1016/j.cej.2007.02.007.
- [25] L. Luo, F. Liu, Y. Xu, J. Yuan, Hydrodynamics and mass transfer characteristics in an internal loop airlift reactor with different spargers, Chem. Eng. J. 175 (2011) 494–504, https://doi.org/10.1016/j.cej.2011.09.078.
- [26] B. Jajuee, A. Margaritis, D. Karamanev, M.A. Bergougnou, Mass transfer characteristics of a novel three-phase airlift contactor with a semipermeable membrane, Chem. Eng. J. 125 (2006) 119–126, https://doi.org/10.1016/j. cei.2006.08.020.
- [27] M.T. Kreutzer, F. Kapteijn, J.A. Moulijn, S. Ebrahimi, R. Kleerebezem, M.C.M. Van Loosdrecht, Monoliths as Biocatalytic Reactors: Smart Gas—Liquid Contacting for Process Intensification, Ind. Eng. Chem. Res. 44 (2005) 9646–9652, https://doi. org/10.1021/je050286m.
- [28] J. Rocha-Rios, N.J.R. Kraakman, R. Kleerebezem, S. Revah, M.T. Kreutzer, M.C. M. van Loosdrecht, A capillary bioreactor to increase methane transfer and oxidation through Taylor flow formation and transfer vector addition, Chem. Eng. J. 217 (2013) 91–98, https://doi.org/10.1016/j.cej.2012.11.065.
- [29] S. Shahhoseyni, M. Rahmani, A. Sivaram, Advanced modeling techniques for predicting gas holdup in bubble columns using machine learning, Fuel 388 (2025) 134449, https://doi.org/10.1016/j.fuel.2025.134449.
- [30] W.A.J. Van Benthum, R.G.J.M. Van Der Lans, M.C.M. Van Loosdrecht, J.J. Heijnen, Bubble recirculation regimes in an internal-loop airlift reactor, Chem. Eng. Sci. 54 (1999) 3995–4006, https://doi.org/10.1016/s0009-2509(99)00097-4.
- [31] S. Nedeltchev, Updated review on the available methods for measurement and prediction of the mass transfer coefficients in bubble columns, Fluids 10 (2025) 29, https://doi.org/10.3390/fluids10020029.
- [32] O.N. Manjrekar, M. Hamed, M.P. Dudukovic, Gas hold-up and mass transfer in a pilot scale bubble column with and without internals, Chem. Eng. Res. Des. 135 (2018) 166–174, https://doi.org/10.1016/j.cherd.2018.05.008.
- [33] Z.-K. Gao, Y.-X. Yang, L.-S. Zhai, M.-S. Ding, N.-D. Jin, Characterizing slug to churn flow transition by using multivariate pseudo Wigner distribution and multivariate multiscale entropy, Chem. Eng. J. 291 (2016) 74–81, https://doi.org/10.1016/j. cei.2016.01.039.
- [34] X. Li, Y. Chen, Z. Zheng, M. Gao, Z. Wang, K. Zhang, H. Liu, X. Zhan, Power-saving airlift bioreactor with helical sieve plates: Developmental and performance studies, Chem. Eng. Res. Des. 158 (2020) 1–11, https://doi.org/10.1016/j. cherd 2020 03 014
- [35] R. Petříček, T. Moucha, F.J. Rejl, L. Valenz, J. Haidl, T. Čmelíková, Volumetric mass transfer coefficient, power input and gas hold-up in viscous liquid in mechanically agitated fermenters. Measurements and scale-up, Int. J. Heat Mass Transf. 124 (2018) 1117–1135, https://doi.org/10.1016/j. iiheatmasstransfer 2018 04 045
- [36] J.C. Rosa, A.B. Neto, C.O. Hokka, A.C. Badino, Influence of dissolved oxygen and shear conditions on clavulanic acid production by Streptomyces clavuligerus, Bioprocess Biosyst. Eng. 27 (2005) 99–104, https://doi.org/10.1007/s00449-004-0386-9.
- [37] S.S. De Jesus, J. Moreira Neto, R. Maciel Filho, Hydrodynamics and mass transfer in bubble column, conventional airlift, stirred airlift and stirred tank bioreactors, using viscous fluid: A comparative study, Biochem. Eng. J. 118 (2017) 70–81, https://doi.org/10.1016/j.bej.2016.11.019.
- [38] V. Lambauer, R. Kratzer, Lab-scale cultivation of Cupriavidus necator on explosive gas mixtures: carbon dioxide fixation into polyhydroxybutyrate, Bioengineering 9 (2022) 204, https://doi.org/10.3390/bioengineering9050204.
- [39] K. Tanaka, A. Ishizaki, T. Kanamaru, T. Kawano, Production of poly(D -3-hydroxybutyrate) from CO₂, H₂, and O₂ by high cell density autotrophic cultivation of *Alcaligenes eutrophus*, Biotech & Bioengineering 45 (1995) 268–275, https://doi.org/10.1002/bit.260450312.
- [40] I. A., T. K., T. N., Microbial production of poly- D- 3-hydroxybutyrate from CO 2, Appl. Microbiol. Biotechnol. 57 (2001) 6–12, https://doi.org/10.1007/ s002530100775.
- [41] A. Santin, T. Spatola Rossi, M.S. Morlino, A.P. Gupte, L. Favaro, T. Morosinotto, L. Treu, S. Campanaro, Autotrophic poly-3-hydroxybutyrate accumulation in Cupriavidus necator for sustainable bioplastic production triggered by nutrient starvation, Bioresour. Technol. 406 (2024) 131068, https://doi.org/10.1016/j. biortech.2024.131068.
- [42] N.J.R. Kraakman, J. González-Martín, C.S. Garcia, S. Cantera, R. Lebrero, R. Muñoz, Multi-channel capillary bioreactor for hydrophobic VOC and CO2 abatement – Process intensification through silicone oil addition, J. Environ. Chem. Eng. 12 (2024) 113695, https://doi.org/10.1016/j.jece.2024.113695.
- [43] M. Turan, Membrane Fouling and Control Approaches in Membrane Bioreactor Systems: A Review, Water Air Soil Pollut. 236 (2025), https://doi.org/10.1007/ s11270-025-07794-6.
- [44] Biotechnology for Plant Protein Production, in: The Future of Plant Protein, Springer Nature Singapore, Singapore, 2025, pp. 99–120, https://doi.org/ 10.1007/978-981-96-4190-1_5.